Extended Abstracts of the 2018 International Conference on Solid State Devices and Materials, Tokyo, 2018, pp379-380

# $MnO_2$ nanorods/reduced graphene oxide composite for aqueous zinc ion battery cathode application

Jiuwei Liu, Yuan Huang, Jiyan Zhang and Hang Zhou

Shenzhen Key Lab of Thin Film Transistor and Advanced Display,
Peking University Shenzhen Graduate School, Peking University, Shenzhen 518055, China
Phone: +86-755-2603-6997 E-mail: zhouh81@pkusz.edu.cn

**Abstract**

**A binder free composite electrode of $MnO_2$ nanorods/reduced graphene oxide with high $MnO_2$ mass ratio (85 wt% of $MnO_2$) is demonstrated using vacuum filtration. Enhanced capacity and improved rate capability are achieved in the $MnO_2$ nanorods/reduced graphene oxide composite electrode for zinc ion batteries application, when compared to the conventional $MnO_2$ electrodes. The $MnO_2$ nanorods/reduced graphene oxide composite electrode exhibits high capacity (251.4 mA h $g^{-1}$ at 0.15 A $g^{-1}$) and good rate capability (157.8 mA h $g^{-1}$ at 3.0 A $g^{-1}$).**

## 1. Introduction

Aqueous zinc ion batteries (ZIBs) have received incremental attention because of high safety, environmental friendliness and abundance of Zn source [1-5]. $MnO_2$ is a most promising cathode material for ZIBs due to its high output voltage and low cost. However, it suffers from low electronic conductivity, which results in sacrificed capacity and low rate performance of the cathode [6-8]. Conventionally, introducing conducting additives (such as carbon black, super P, carbon nanotube, or PEDOT with mass ratio ranging from 20%-33%) would help to improve the electronic conductivity of the $MnO_2$-based electrode [8-10]. On the other hand, binders (such as polyvinylidene fluoride or carboxymethyl cellulose with mass ratio around 10%) are required to construct a workable cell. Finding efficient additives that enhances the electronic conductivity of $MnO_2$, while at the same time minimizing the content of both additives and binders, become a tempting goal as it would lead to high performance electrode with high packing density. Herein, we adopt vacuum filtration to deposit $MnO_2$ nanorods and reduced graphene oxide (rGO) sheets onto the carbon cloth. We obtained a flexible and binder-free composite electrode of $MnO_2$ nanorods/reduced graphene oxide (rGO) with high $MnO_2$ mass ratio (85 wt% of $MnO_2$). Enhanced capacity, improved rate capability and cycling stability are achieved in the $MnO_2$ nanorods/rGO composite electrodes, when compared to the conventional $MnO_2$ electrodes.

## 2. Experiments

The $MnO_2$ nanorods were synthesized by a hydrothermal method. 0.1264 g $KMnO_4$ and 1 mL sulfuric acid were homogeneously mixed with 79 mL distilled water. The solution was then poured into a Teflon-lined reactor and was subjected to hydrothermal condition at 140 °C for 12 h. Then, the resulting powder was filtered and washed with plenty of distilled water. Finally, the filtered powder was dried in a vacuum oven at 60 °C for 2 h, following an annealing process at 300 °C for 1 h under air atmosphere. The $MnO_2$/rGO composite electrodes were prepared using a vacuum filtration method. 12 mg $MnO_2$ nanorods and 2.1 mg rGO were dispersed in 3 mL isopropyl alcohol (IPA) by sonication for 2 h, and then mixed to form a uniform suspension. The suspension was filtered through carbon cloth on the top of a filter paper, via vacuum filtration. Finally, the composite electrode was dried in a vacuum oven at 60 °C for 2 h. The zinc was electrodeposited on carbon cloth as counter electrode [9]. 2 M $ZnSO_4$ with 0.1 M $MnSO_4$ aqueous solution was used as electrolyte.

## 3. Results and discussions

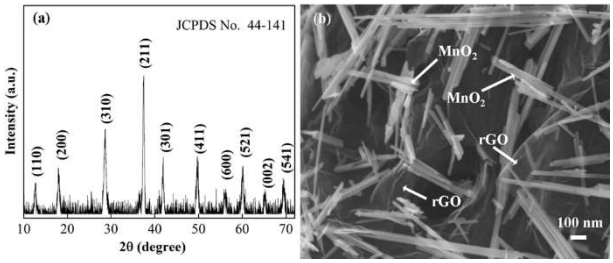


Fig. 1 a) XRD spectrum of $MnO_2$ sample. b) SEM image of the $MnO_2$/rGO composite sample.

XRD result of $MnO_2$ samples is shown in Figure 1a. All diffraction peaks can be indexed to the crystalline phase of α-$MnO_2$ (JCPDS: 44-0141). The SEM image of $MnO_2$ nanorods/rGO (Figure 1b) shows that the α-$MnO_2$ nanorods are about 50~100 nm in width and 1~2 μm in length. $MnO_2$ nanorods and rGO are uniformly distributed on carbon cloth.

The electrochemical properties of the $MnO_2$/rGO electrodes with a mass ratio of 85:15 have been compared to those of the conventional $MnO_2$ electrode (70 wt% $MnO_2$ nanorods, 20 wt% Super P, and 10 wt% PVDF binder). Figure 2a shows cyclic voltammetry curve of the $MnO_2$/rGO and conventional $MnO_2$ electrodes at a scan rate of 0.2 mV $s^{-1}$ in voltage range of 1.0-1.9 V vs. $Zn^{2+}$/Zn. For conventional $MnO_2$ cathode, two separated reversible redox peaks (reduction peaks: 1.22 and 1.34 V, oxidation peak: 1.60 and 1.64 V) can be clearly observed, corresponding to a two-step reaction. The reaction mechanism for $MnO_2$ has been reported previously that the $MnO_2$ cathode experiences a consequent $H^+$ and $Zn^{2+}$ insertion/extraction process during the

discharging/charging [11]. The $MnO_2$/rGO sample shows similar oxidation/reduction peaks during the anodic/cathodic scan, indicating that the rGO additive did not affect the redox reactions in the $MnO_2$ electrode. Nevertheless, the magnitudes of their current density of peaks are different. The $MnO_2$/rGO electrodes show higher peaks than the conventional $MnO_2$ electrodes, indicating its higher capacity than the conventional $MnO_2$ electrodes.

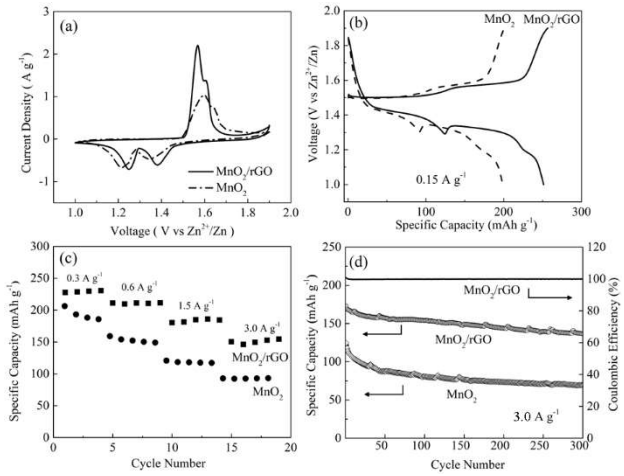


Fig. 2 a) Cyclic voltammogram of the $MnO_2$/rGO and conventional $MnO_2$ electrodes. b) Comparison of the charging and discharging profiles of the samples at the current density of 0.15 A $g^{-1}$. c) Specific capacities of the samples at various current density. d) Cycling stability of the samples cycled at 3.0 A $g^{-1}$ and corresponding Coulombic efficiency of $MnO_2$/rGO electrode.

Figure 2b compares the charging and discharging profiles of the samples at the current density of 0.15 A $g^{-1}$. Both batteries present two similar discharge plateaus, which are attributed to consequent $H^+$ and $Zn^{2+}$ insertion process. However, the discharging capacity of the $MnO_2$/rGO electrodes at 0.15 A $g^{-1}$ is significant higher (~ 251.4 mA h $g^{-1}$) than that of the conventional $MnO_2$ electrode (~201.0 mA h $g^{-1}$). This result is consistent with the CV profiles in Figure 2a. Figure 2c shows comparison of the rate performance of the $MnO_2$/rGO and conventional $MnO_2$ electrodes. It is obvious that the $MnO_2$/rGO composite electrode exhibits superior rate capability when compared to the conventional $MnO_2$ electrode. For example, the $MnO_2$/rGO sample can deliver discharging capacity of ~223.0 mA h $g^{-1}$ at low rate of 0.3 A $g^{-1}$. A Little decrease in the discharging capacity is observed when the rate is increased to 0.6 A $g^{-1}$, and is kept at ~157.8 mA h $g^{-1}$ at further rate increase to 3.0 A $g^{-1}$. As a comparison, the conventional $MnO_2$ electrodes exhibits much lower discharge capacity, that is, ~203.2 mA h $g^{-1}$ even at low discharge rate of 0.3 A $g^{-1}$, and further drops to ~93.9 mA h $g^{-1}$ at 3.0 A $g^{-1}$.

The cycling performance of the $MnO_2$/rGO sample is also improved especially at high rates when compared to conventional $MnO_2$ samples (Figure 2d). More than 80% of its initial capacity and high Coulombic efficiency (>99.7%) still remained even the cyclic number extended to 300 cycles at high current density of 3.0 A $g^{-1}$, indicating the excellent cycling stability of the $MnO_2$/rGO composite sample. As a comparison, the capacity retention of the conventional $MnO_2$ sample at 3.0 A $g^{-1}$ (after 300 cycles) is 57%.

## 3. Conclusions

In summary, $MnO_2$ nanorods/rGO composites have been successfully fabricated by a vacuum filtration process, which results in a flexible and binder free cathode for ZIBs. When compared to conventional $MnO_2$ cell, the $MnO_2$/rGO composite cathode shows largely enhanced capacity, excellent rate capability and cycling stability. The $MnO_2$ nanorods/rGO composite electrodes exhibits high capacity (251.4 mA h $g^{-1}$ at 0.15 A $g^{-1}$) and good rate capability (157.8 mA h $g^{-1}$ at 3.0 A $g^{-1}$). With the excellent device performance, the ease of fabrication, such Zn-$MnO_2$/rGO batteries are very promising for use as wearable energy storage devices.


## Acknowledgements

This work is supported by the China Postdoctoral Science Foundation funded project (2017M620517), and the Shenzhen Science and Technology Innovation Committee (No. JCYJ20170412150411676, and JCYJ20170818090257257).


## References


[1] N. Zhang, F. Cheng, J. Liu, L. Wang, X. Long, X. Liu, F Li, J. Chen, Nat Commun. 2017, 8, 405.

[2] N. Zhang, F. Cheng, Y. Liu, Q. Zhao, K. Lei, C. Chen, X. Liu, J. Chen, J. Am. Chem. Soc. 2016, 138, 12894.

[3] P. He, M. Yan, G. Zhang, R. Sun, L. Chen, Q. An, L. Mai, Adv. Energy Mater. 2017, 7, 1601920.

[4] C. Xia, J. Guo, Y. Lei, H. Liang, C. Zhao, H. N. Alshareef, Adv. Mater. 2017, 1705580.

[5] P. He, G. Zhang, X. Liao, M. Yan, X. Xu, Q. An, J. Liu, L. Mai, Adv. Energy Mater. 2018, 1702463

[6] M. H. Alfaruqi, S. Islam, V. Mathew, J. Song, S. Kim, D. P. Tung, J. Jo, S. Kim, J. P. Baboo, Z. Xiu, J. Kim, Appl. Surf. Sci. 2017, 404, 435.

[7] W. Qiu, Y. Li, A. You, Z. Zhang, G. Li, X. Lu, Y. Tong, J. Mater. Chem. A 2017, 5, 14838.

[8] D. Xu, B. Li, C. Wei, Y.-B. He, H. Du, X. Chu, X. Qin, Q.-H. Yang, F. Kang, Electrochim. Acta 2014, 133, 254.

[9] Y. Zeng, X. Zhang, Y. Meng, M. Yu, J. Yi, Y. Wu, X. Lu, Y. Tong, Adv. Mater. 2017, 29, 1700274.

[10] B. Wu, G.n Zhang, M. Yan, T. Xiong, P. He, L. He, X. Xu, L. Mai, Small 2018, 14, 1703850.

[11] W. Sun, F. Wang, S. Hou, C. Yang, X. Fan, Z. Ma, T. Gao, F. Han, R. Hu, M. Zhu, C. Wang, J. Am. Chem. Soc. 2017, 139, 9775.